Science Translational Medicine
AAAS

stm.sciencemag.org/cgi/content/full/12/531/eaay4006/DC1

Supplementary Materials for

A geometrically adaptable heart valve replacement

Sophie C. Hofferberth*, Mossab Y. Saeed, Lara Tomholt, Matheus C. Fernandes, Christopher J. Payne, Karl Price, Gerald R. Marx, Jesse J. Esch, David W. Brown, Jonathan Brown, Peter E. Hammer, Richard W. Bianco, James C. Weaver, Elazer R. Edelman, Pedro J. del Nido*

*Corresponding author. Email: sophie.hofferberth@cardio.chboston.org (S.C.H.); pedro.delnido@cardio.chboston.org (P.J.d.N.)

Published 19 February 2020, *Sci. Transl. Med.* **12**, eaay4006 (2020)
DOI: 10.1126/scitranslmed.aay4006

The PDF file includes:

Other Supplementary Material for this manuscript includes the following:

(available at stm.sciencemag.org/cgi/content/full/12/531/eaay4006/DC1)

Movie S1 (.mp4 format). A geometrically adaptable heart valve replacement.
Data file S1 (Microsoft Excel format). Primary data.

Materials and Methods

Characterization of venous valve geometry

To create the venous valve-inspired leaflet geometry, we studied the morphology of native human venous valves, obtained from commercial sources. We took measurements from cryopreserved human femoral (N = 1) and saphenous vein (N = 1) grafts (CryoLife Inc., Kennesaw, GA) (fig. S1A). The native diameter of the femoral and saphenous vein specimens was 8 mm and 3 mm, respectively. Each vein graft specimen contained multiple valves (femoral vein, N = 2; saphenous vein, N = 2).

The cryopreserved vein grafts were initially thawed in a warm water bath. Specimens were then incised longitudinally, and the location of each valve was confirmed (fig. S1B). Valve dimensions were measured in the non-distended state (fig. S1C). Valve height, defined as the linear distance from the top of the valve commissure (where leaflets meet and insert into the vessel wall) to the base of the leaflet, valve diameter, and leaflet mid-height (linear distance from top of valve commissure to nadir of leaflet free edge) were measured for each venous valve (N = 4) (fig. S1C). Mean values were calculated for each dimension across all specimens. The geometry of the 3-dimensional leaflet-vessel wall attachment curve was also recorded for each valve specimen (fig. S1C).

Mean valve height to diameter ratio was 2.03:1 ± 0.06 and mean leaflet mid-height to commissural height ratio was 0.495:1 ± 0.02 (table S1). The morphology and dimensions of the native venous valve specimens were used to design the leaflet geometry of the biomimetic primary valve prototype (fig. S1D).

Generation of biomimetic bileaflet valve geometry

The three key geometric features of the biomimetic valve design are: i) the leaflet profile geometry, ii) the 3-dimensional leaflet attachment geometry, and iii) the valve expansion geometry. We developed methods for geometrically describing these features based on two parameters: the valve height (H) and the valve diameter (D). Digitized geometry was generated in a solid modeling computer aided design (CAD) software SolidWorks (Dassault Systèmes).

Leaflet profile geometry

The leaflet profile geometry was defined as a 2D geometric profile that was created based on the morphology and dimensions observed in human venous valve specimens (fig. S1). For a given valve, the leaflet profile was scaled such that the commissure-to-commissure length is defined as half the valve circumference ($0.5\pi D$) and the commissure-to-base length is equivalent to the valve height (H). The leaflet mid-height (L_H) was defined as 0.5H in accordance with human venous valve dimensions (fig. S2A).

Leaflet attachment geometry

We defined the leaflet attachment geometry as the geometric profile created by the native venous valve leaflet joining to the surrounding vessel wall. This attachment geometry can be approximated as a three-dimensional (3D) curve. To obtain this curve profile, we projected an elliptical quadrant onto a cylinder, which represents the inner wall of a vessel (fig. S2B).

The ellipse profile had a semi-major axis length equivalent to the height of the valve (H) and a semi-minor axis with a length equivalent to the radius (r) of the valve. The cylinder had a radius equivalent to that of the valve. The ellipse was then normally projected onto the cylinder; the ellipse co-vertex was made to be coincident with the cylinder centerline and the ellipse vertices and center were all coincident with the outer edge of the cylinder when viewed from the side projection (fig. S2B). The resulting 3D curve projections were mirrored about the centerline of the cylinder to generate the attachment geometry for the second leaflet.

Expanding valve geometry

We developed a methodology for diametrically expanding the valve leaflet attachment geometry to approximate radial expansion of a growing artery/valve annulus. We fixed the perimeter length of the 3-dimensional leaflet attachment curve (s) so that radial expansion was accompanied by a reduction in valve height (fig S3A). The varying aspect ratio leaflet attachment geometry is a critical feature of our biomimetic valve design. We firstly defined a baseline leaflet attachment geometry for a baseline height (HB) and a baseline diameter (DB). Next, we computed the curve length of the baseline leaflet attachment curve (s). We then generated expanded valve geometries by computing the valve height (H) from the expanded diameter (D) and fixed length of the leaflet attachment curve (s). Fig. S3B shows the decreasing height-to-diameter ratio (H/D) for an expanding valve from initial diameter DB to the largest expansion diameter at which a given valve geometry stays functional. The plots represent valve geometries with various baseline HB/DB ratios, including 2, 1.7 and 1.5.

Optimal valve height-to-diameter ratio for pediatric patients

Our goal was to design a size-adjustable prosthetic heart valve with dimensions suitable for implantation from infancy through to adulthood. To determine these design parameters, we investigated the critical anatomic dimensions of the youngest pediatric patients who require heart valve replacement. Tetralogy of Fallot (ToF) is the most common congenital right heart defect and accounts for nearly 10% of all children born with heart anomalies (*1*). The native pulmonary valve in ToF is usually abnormal and prohibits normal outflow of blood to the lungs. The serious morbidity of this defect necessitates surgical correction in the first few months of life, however current approaches fail to preserve pulmonary valve function. Thus, our valve dimensions (height and diameter) needed to be suitable for implantation in ToF patients undergoing surgical repair in early infancy.

Since the native pulmonary valve annulus diameter is generally severely hypoplastic (undersized) in ToF patients, we referenced population-based echocardiographic data to determine the optimum baseline valve diameter. These data indicate that a normal sized pulmonary valve annulus diameter is approximately 10 mm in a 3-month-old child (*23*), which we used as the baseline valve internal diameter for subsequent investigations.

To determine the optimum valve height-to-diameter ratio, we measured the length of the main pulmonary artery in a cohort of ToF patients who underwent surgical repair at Boston Children's Hospital. Institutional Review Board approval was obtained, and a waiver of

documented patient consent was granted. We performed a retrospective echocardiographic analysis in 22 patients, aged less than 6 months, who underwent primary repair of ToF at Boston Children's Hospital between August 2014 and August 2016.

Imaging of the right ventricular outflow tract and pulmonary artery was performed using standard echocardiographic views (*52-54*) (fig. S4A). A single reviewer independently obtained measurements from the pre-operative 2 dimensional (2D) transthoracic echocardiogram (TTE) in all patients. A second independent and blinded reviewer measured a random sample. All echocardiographic measurements were analyzed using Image-Arena software (versions 4.6; Tom-Tec Imaging Systems). Main pulmonary artery length was defined as the linear distance between the pulmonary valve annulus and the bifurcation (branch point) of the left and right pulmonary arteries (fig. S4B), and the anatomic location of the pulmonary artery bifurcation was confirmed by color flow imaging in the same view (fig. S4C). The measurement was performed 3 times in each patient and the mean value was recorded. Among the 22 patients, mean age was 89.6 ± 29 days and mean length of the main pulmonary artery was 17.9 ± 2.8 mm.

Based on this data, the maximum acceptable prosthesis height is 17 mm for this particular population of infant patients. Thus, given a baseline valve diameter of 10 mm, we determined a suitable valve aspect ratio for pediatric patients is 1.7:1.

Leaflet material selection and characterization

We sought a leaflet material with limited compliance (inextensible) to mimic mechanical properties of the native venous valve leaflet and test our hypothesis that a varying aspect ratio valve design enables radial expansion without necessitating an increase in leaflet surface area. We therefore chose 0.1 mm thickness expanded polytetrafluoroethylene (ePTFE) (Gore Preclude pericardial membrane, W. L. Gore & Associates) as the model leaflet material for our biomimetic valve prototype. This material was chosen because ePTFE is biocompatible, relatively inextensible, and is currently used for intra-cardiac procedures. We performed biaxial mechanical testing to quantify material extensibility and anisotropy.

A 5-N capacity biaxial testing device (Biotester, CellScale) was used to perform mechanical testing of the 0.1 mm ePTFE material (fig. S5A, B).

Identification of material orientation

To identify principal material orientation, a square section of material was cut from a 15 cm x 20 cm sheet of commercial 0.1 mm thickness ePTFE. The employed mechanical testing protocol was the same as previously described by our group (*55*) and outlined below.

Samples were cut into 10 mm x 10 mm squares (fig. S5C), and material thickness was confirmed in 3 regions across each sample using an electronic thickness gauge (Model CD-68CT, Mitutoyo). Samples were affixed to four tungsten rakes, and each rake was fitted with 5 tines spaced at 1.0 mm (fig. S5C). The resulting test specimens were then immersed in a temperature-controlled (37 °C) bath to emulate in vivo conditions.

Experimental protocol

A biaxial testing protocol was developed using the Biotester equipment software (LabJoy). The LabJoy data acquisition module was utilized to set i) the parameters for the test phase of each load cycle, ii) the water bath temperature, and iii) the data and image acquisition rate (15 Hz). The test protocol involved application of preload to samples, stretch, hold, recovery, and rest. Biaxial testing was performed with the Biotester system in force-control mode (fig. S5D).

To approximate physiologic valve loading conditions, we tested samples at a maximal loading condition of 1 N, and each sample was subjected to preconditioning cycles prior to evaluation. Samples were initially subjected to 10 cycles of equibiaxial stretch at 1 N, followed by seven proportional biaxial cycles at load ratios (Y:X) of 0.25:1, 0.5:1.0, 0.75:1.0, 1.0:1.0, 1.0:0.75, 1.0:0.5, 1.0:0.25 N (fig. S5D).

Computation of stresses and strains

The strain field across samples was estimated using a combination of the Labjoy software and customized software, as previously described (*56*).

Fabrication of functional valve samples

Valve samples were fabricated based on the leaflet profile geometry and leaflet attachment geometry methodologies described above. To fabricate working valve samples, manufacturable leaflet attachment frames were designed using CAD software. Leaflet attachments were then generated using a sweep feature that combined the 3D leaflet attachment curve and a circular cross section (Ø2.5 mm) to generate a solid volume that could be fabricated via additive manufacturing. The leaflet attachment geometry was based on the inner diameter of the frame samples to ensure that the H/D ratio was representative of the leaflet attachment location irrespective of the frame thickness (fig. S6). A series of holes were patterned along the swept feature to allow leaflets to be physically sewn into the leaflet attachment frame. During the early design stages, sequential prototype evaluation was performed using models fabricated with a Form2 stereolithography-based 3D printer (FormLabs), using their RS-F2-TOTL-05 (Tough) resin. Once a final geometry had been identified, subsequent physical prototypes were fabricated from ASTMF1537-11 cobalt chrome using direct metal laser sintering additive manufacturing (MLab, Concept Laser GmbH).

Leaflets were cut from a 0.1 mm thickness sheet of ePTFE (Gore Preclude pericardial membrane, W. L. Gore & Associates) using surgical scissors and a guiding template. The leaflets were cut out such that the most extensible material orientation was oriented parallel to the long axis of the leaflet (fig. S6).

Leaflets were sewn into the leaflet attachment frame with a running stitch. The leaflets were initially sewn at the commissure and valve base locations to ensure correct alignment. Finally, the assembled valve samples were placed inside flexible polyurethane tubing (Tygon, Saint-Gobain). A thin film of sealant (Sil-poxy) was manually applied to the underside of the leaflet attachment frames to ensure no paravalvular leakage during hydrodynamic testing.

In vitro hydrodynamic testing

Benchtop hydrodynamic performance testing was used to determine whether our biomimetic bileaflet valve design with i) fixed leaflet attachment perimeter length and ii) fixed leaflet profile geometry, could function effectively with diametric expansion. A comprehensive series of experiments were performed to characterize transvalvular pressure gradient (pressure drop), effective orifice area (EOA), and valve regurgitation over a wide range of physiologic and supraphysiologic flow and pressure conditions.

Flow loop apparatus

Valve prototypes were tested in a pulsatile flow loop apparatus (ViVitro Labs Inc). This system complies with ISO standards for surgical cardiac valve prostheses (ISO 5840-2:2015) and transcatheter valves (ISO 5840-3:2013). The flow loop system (fig. S7) was powered by a volume-displacement piston pump (Superpump, ViVitro Labs Inc) to simulate cardiac output. A mixture of 0.9 ± 0.2 % sodium chloride in glycerin and distilled water with a viscosity of 3.0 ± 0.5 cP [0.5 ± 0.5 mL of Cosmocil (Londa) per 1L] was used as a working fluid to emulate blood.

The pump displaced the working fluid into a chamber that incorporated a sealed silicone ventricular sac, causing compression of the ventricular sac to mimic cardiac muscle function. Repeated compression and distention of the ventricular sac generated a pulsatile flow in the flow loop apparatus. A reservoir emulating the right atrium was connected to the ventricular sac, and a one-way mechanical valve at this inlet was utilized to mimic the atrioventricular valve (mitral/tricuspid valves). A pressure transducer (HCM018, ViVitro Labs Inc) was mounted in the atrial reservoir to monitor atrial pressure. An outlet chamber from the ventricular sac provided the testing chamber for the valve prototype. A pressure transducer (HCM018, ViVitro Labs Inc) and electromagnetic flow probe (EP688, Carolina Medical) were mounted proximal to where the valve prototype was mounted. A second pressure transducer (HCM018, ViVitro Labs Inc) was mounted distal to the valve prototype. High frame rate cameras (Photron SA3 60K M2) were used to image the valve prototypes in the transverse plane and from a plan view at a rate of 1000 fps. The working fluid was pumped from the ventricular sac, through the prototype valve, then looped back to the atrial reservoir via a network of tubing that had adjustable hydrodynamic resistance to represent the body. Air volumes were used to add compliance to an otherwise rigid system to replicate anatomical compliance. Fluid was regulated at 37±0.1 °C using a heat exchanger system. The pumping parameters were adjusted by a control system to allow systematic testing of valve prototypes and specific hemodynamic conditions. The target forward flow volume per cycle, beat rate and systolic duration period (as a fraction of a cardiac cycle) were each adjustable. The systolic and diastolic arterial pressures were also adjusted; similarly, the back pressure on the valve prototype was adjustable by changing the peripheral resistance and compliance volumes. Experimental data was processed by a data acquisition system (ViViTest, ViVitro Labs Inc) at a rate of 256 samples per beat (60 beats/min sampling is 256 Hz and 150 beats min is 102 Hz).

Output metrics

The purpose of these in vitro experiments was to quantitatively assess transvalvular pressure gradient, EOA, and valve regurgitation for the geometrically adaptable bileaflet valve design.

The first output metric of interest is the peak-to-peak transvalvular pressure gradient. This is defined as the pressure difference between the ventricular peak pressure and the arterial peak pressure (peak pressure downstream of valve). This pressure metric is of interest because it assesses how effectively the valve achieves unimpeded forward flow, i.e an indicator of heart valve efficiency.

We also assessed the EOA of each valve sample during operation to assess how effectively the biomimetic valve design accommodates radial expansion without obstructing forward flow. The EOA provides an index of how well a valve design utilizes its internal stent orifice area. An effective orifice area was computed using a 1D incompressible, steady-state fluid flow model, defined as:

$$\text{EOA } (\text{cm}^2) = \frac{Qrms}{51.6\sqrt{\frac{\Delta P}{\rho}}}$$

Where Q_{rms} is the root mean square systolic/diastolic flow rate (cm^3/s), ΔP is the mean systolic/diastolic pressure drop (mmHg), and ρ is the working fluid density.

Valve regurgitation is a metric of interest because it demonstrates the extent to which a valve obviates flow reversal and effectively acts as a one-way valve. Valve regurgitation was quantified in absolute terms as a volume of regurgitant flow, which incorporates the sum of the valve closing volume and the valve leakage volume. Valve closing volume is defined as the volume of reverse flow through the valve during valve closure, and valve leakage volume represents the volume of reverse fluid flow that occurs through the valve after valve closure. Valve regurgitation was also considered in relative terms, as a % fraction of fluid forward flow through the valve.

For each test condition, output metrics were acquired for a total of 10 consecutive cardiac cycles at steady-state conditions.

Experimental variables

The primary dependent variables in these in vitro characterization studies were the expanding valve geometry from an initial baseline valve diameter and the initial H/D ratio. A series of 11 samples were fabricated in total using the methods described above. An initial 5 samples were fabricated with a baseline H/D=1.7 and baseline internal diameter (ID) of 16 mm. Valve prototypes were fabricated at baseline (1X) and expanded dimensions in +20% increments up to 1.8X diameter, with the following dimensions: 16 mm (baseline), 19.2, 22.4, 25.6, and 28.8 mm. A further 6 samples of baseline H/D=2 and 16 mm baseline ID were also fabricated at +20% increments (diameters of 16 mm, 19.2, 22.4, 25.6, 28.8 mm and 32 mm). These particular valve sample diameters and increments were chosen to match standardized flexible polymer tubing diameters compatible with the experimental flow loop apparatus. For each expanding series of valve prototypes, the leaflet profile geometry sewn into each leaflet attachment frame was identical to mimic a non-growing leaflet. The leaflet profile geometry for each series of samples was defined by the baseline valve H/D ratio.

For each valve sample of a given geometry and dimension, we further manipulated key hydrodynamic input parameters to characterize each sample across a range of physiological and super-physiological conditions. Since the primary objective of the geometrically adaptable bileaflet valve design was to successfully accommodate diametric vessel growth

without loss of function, we derived hemodynamic flow rates appropriate for each valve sample according to its diameter. Since cardiac output (blood flow rate) varies considerably between humans of different ages (and thus valves of different diameter), we characterized samples by maintaining a constant cardiac index. Cardiac index is a hemodynamic parameter that relates the cardiac output to the size of an individual with respect to body surface area. To calculate the cardiac output for a given valve diameter, we obtained an average body surface area for the relevant valve diameter using clinical data (*23, 56*). Secondly, we computed the cardiac output for a given valve diameter from the estimated body surface area and a target cardiac index.

To assess the transvalvular pressure gradient (pressure drop) and the EOA across each valve dimension, we assessed 3 cardiac indices: 2.5, 3.0, and 3.5 to represent a broad physiologic range. During each test, we fixed the systolic duration period to 45% (±5%); Pressures were adjusted to assess valve performance under right and left heart conditions; mean arterial pressure ranged from 20 mmHg to 100 mmHg, systolic arterial pressure ranged from 25 mmHg to 200 mmHg, and diastolic arterial pressure ranged from 10 to 160 mmHg. Beat rates ranged from 60 to 150 bpm.

To assess valve regurgitation, we fixed the cardiac index to be 3.0. For each valve sample, we varied both the heart rate (60, 80, and 150 bpm) and the back pressure (diastolic pressure) on the valve (5, 10, 20, 50 80, 160 mmHg). During these tests we fixed the systolic duration period to be 45% of the cardiac cycle (±5%).

Finite element modeling

In this section, we describe the construction and processing of the Finite Element Analysis (FEA) performed to evaluate the magnitude and distribution of stresses on the geometrically adaptable valve leaflet in a quasi-static, closed position (diastole). The leaflet-stent model was constructed using the commercial Computer Aided Design (CAD) software SolidWorks (Dassault Systèmes) and was designed to precisely match the geometry of the experimental setup. Separate CADs for the leaflet and the different expansion geometry stents were generated. The FEA simulations were performed using the commercial solver ABAQUS/Explicit 2017 (Dassault Systèmes). The stent geometry was assumed to be a non-deformable rigid material with a set of displacement conditions imposed to simulate the transition between the different expansion states. The leaflet geometry was modeled using 3D deformable elements (C3D8R - 8-node hexahedral brick general-purpose continuum elements with reduced integration for finite membrane strains) with TIE constraints imposed on the nodes located along the perimeter of the leaflet. These constraints connect the leaflet to the stent geometry. The mesh size for the leaflet is chosen to remain smaller than 0.4 mm anywhere within the leaflet domain. A general contact condition is defined between all nodes interacting with each other.

The constitutive model used is set to match the material properties of 0.1 mm thickness ePTFE (Gore Preclude pericardial membrane, W.L Gore and Associates, Inc.), which satisfies an isotropic hyperelastic Marlow material. For this material model, the strain energy potential is described by $U = U_{dev}(\bar{I}_1) + U_{vol}(J_{el})$, where U is the strain energy per unit of reference volume, with U_{dev} as its deviatoric part and U_{vol} as its volumetric part; $\bar{I}_1$ is the

first deviatoric strain invariant and J_{el} is the elastic volume ratio. We obtained the parameters for this material model by fitting the model to the experimental data. We chose our material model to be within 2 standard deviations of the most compliant material direction to match the physical deformation of the valve leaflets observed under in vitro flow loop testing conditions. This was chosen with the rationale to provide the most appropriate isotropic measure given that the experimental leaflet had the more compliant ePTFE material direction aligned with the direction of largest strain. Additionally, to create a computationally efficient model, we used mass-scaling to arrive at the desired quasi-static solution while introducing negligible numerical errors.

The FEA model is subdivided into two sequential steps: the first step expands the base geometry stent to achieve the desired expansion state. This step is performed by creating a map between the different expansion states and applying a smooth expansion transition between the different states. A map is created that relates the transition for each node from its original state to its expanded state. This map is then applied as a displacement condition for each of the nodes. Once the final desired expansion configuration is achieved, a subsequent step applies the pressure boundary condition on the leaflet. The negative pressure conditions are imposed along the outflow surface of the leaflets, leading the leaflets to close and interact. The pressure step is slowly imposed as a ramping step to minimize the kinematics of the model and efficiently arrive at the steady-state, quasi-static solution. For each FEA simulation, the model is simulated long enough to ensure the correct quasi-static deformation solution matching the experimental deformation is achieved. Furthermore, a calibrated damping coefficient is applied to minimize numerical kinematics resulting from the model's inertia.

In vivo acute ovine studies: functional assessment of primary biomimetic valve geometry

We performed acute in vivo studies in juvenile sheep to evaluate functional performance of the primary biomimetic valve geometry. The animal experiments were conducted in full compliance with the 1996 Guide for the Care and Use of Laboratory Animals recommended by the U.S. National Institutes of Health. All acute in vivo studies were performed at Boston Children's Hospital. The experimental protocol was approved by the hospital's Institutional Animal Care and Use Committee.

Polymer-based prototypes of the primary valve geometry were fabricated using stereolithography additive manufacturing (Somos, perFORM, DSM Functional Materials), which was performed to enable artifact-free echocardiography of the device. Reinforcement features were added to the prototypes to increase the rigidity of the polymer valve frame. The valve samples generated for in vivo testing were equivalent geometry and dimensions to the in vitro samples tested and were generated using the same methods as previously described.

To determine in vivo functionality of the primary biomimetic valve geometry we tested the two polar states of valve expansion (1X and 1.8X). A total of 8 polymer-based prototypes were produced. Four valves were fabricated with baseline H/D ratio of 1.7:1, and 14 mm internal diameter (ID) and four valves were fabricated with a 1.8X expanded diameter from these baseline dimensions (valve ID = 25 mm). To facilitate surgical implantation, a

sleeve/sewing cuff was constructed using Gore-Tex vascular graft (W.L Gore and Associates, Inc.).

Procedure

Female Dorset lambs (N = 4, mean weight 20.9 ± 2.2 kg, Parsons EM and Sons Inc.) and female Dorset sheep (N = 4, mean weight 58.1 ± 2.7kg, Parsons EM and Sons Inc.) were used. Animals were anesthetized using intravenous (IV) Ketamine (10 mg/kg), versed (0.1 mg/kg) and intramuscular injection (IM) of atropine (0.04 mg/kg). The animals were intubated with a cuffed endotracheal tube and mechanically ventilated with volume-control mode (Fabius Tiro; Draeger Medical, Andover, MA). Anesthesia was maintained with inhaled desflurane (8-12%). A transurethral urinary catheter was placed for monitoring urine output. Arterial and central venous lines were placed percutaneously in the femoral artery and external jugular vein for arterial and central venous pressure monitoring, respectively. Electrocardiogram monitoring was achieved using an esophageal probe and temperature was monitored via rectal probe placement. The neck, chest and groin were disinfected using povidone-iodine and alcohol solutions.

Access to the heart and pulmonary valve was achieved by performing a left-sided thoracotomy in the 4th intercostal space, and external measurements of the pulmonary valve annulus diameter and main pulmonary artery length were performed. Baseline hemodynamic data was obtained via placement of right ventricular and pulmonary artery pressure lines and a perivascular flow probe (Transonics, TS420) around the distal main pulmonary artery. Baseline 2D epicardial echocardiography was performed using a matrix array ultrasound probe X7-2 (2-7 MHz) on an iE33 system (Philips Healthcare) to measure the native pulmonary valve annulus diameter, main pulmonary artery length (defined as the linear distance between the pulmonary valve annulus and bifurcation of the branch pulmonary arteries) and assess overall heart function. After intravenous heparin (300 IU/kg) was administered to achieve an activated clotting time of >350 seconds, arterial cannulation was performed via the ascending aorta and venous cannulation was performed via the right atrial appendage. Cardiopulmonary bypass was initiated using an oxygenator (FX15 or FX25, Terumo Medical Corporation). Isoflurane (1-4%) was administered for maintenance of anesthesia during cardiopulmonary bypass. With the animal cooled to 33°C and under beating-heart conditions, a longitudinal incision was made along the anterior aspect of the main pulmonary artery, extending to just below the level of the pulmonary valve annulus. The native pulmonary valve leaflets were then excised. Next, depending on the animal size, we implanted either a 14 mm or 25 mm internal diameter valve prototype in the native pulmonary valve position. This was performed using interrupted 4-0 Prolene sutures, placed in a circumferential fashion. After valve implantation, the pulmonary artery was closed, and hemostasis was obtained. Animals were then weaned off cardiopulmonary bypass and arterial and venous cannulas were removed. Animals were observed for 4 to 6 hours post wean from cardiopulmonary bypass. 2D epicardial echocardiography, including color and continuous wave Doppler imaging, and 3D echocardiography was performed at 1- and 4-hours post implantation to evaluate valve function. Continuous monitoring of right ventricular and pulmonary artery pressures, and main pulmonary artery flow were also performed throughout the observation period to assess valve hemodynamic performance and overall heart function. At the conclusion of the study, animals were euthanized by intravenous injection of overdosed pentobarbital sodium (Fatal-Plus, 86 mg/kg). The heart was then excised and opened for direct inspection of the valve.

Data analysis

The flow and pressure data were logged using an acquisition system (Powerlab, AD Instruments) at a rate of 10 kHz. Flow and pressure data were analyzed using data analysis software (LabChart, AD Instruments). To assess valve regurgitation, we integrated the flow rate to obtain a forward flow volume, a closing volume and valve leakage volume. The total regurgitant volume (closing and leakage volumes) was then expressed as a % of the forward flow volume. Transvalvular pressure gradient was computed from the measured right ventricle and PA pressures (right ventricular pressure – PA pressure). Peak-to-peak transvalvular pressure gradient values were computed during the forward flow phase.

In vivo acute ovine study: Biomimetic valve implantation in native aortic valve position

For proof of concept, we also conducted acute, non-survival experiments to implant the biomimetic valve prototype in the native aortic valve position of juvenile sheep (N = 2). The goal was to assess mechanical and hemodynamic performance of the biomimetic valve in the left-sided systemic semilunar valve position. The experimental protocol for these experiments was identical to the acute, non-survival pulmonary valve implants.

Expandable biomimetic valve prototype: in vitro expansion and hydrodynamic testing

Biomimetic expandable valve prototypes were fabricated using 0.1mm ePTFE for leaflet material and a laser-cut stainless-steel frame (fig. S13). Fabricated valves were sequentially balloon dilated on the benchtop from 12.5 mm (1X) up to 23 mm (1.8X) (Fig. S13). These prototypes were then tested at 4 states of expansion (12.5 mm ID, 16 mm ID, 20 mm ID and 23 mm ID) in the aforementioned pulsatile flow loop system (Vivitro Labs, pulse duplicator). The purpose of these in vitro experiments was to quantitatively assess transvalvular pressure gradient, EOA, and degree of valve regurgitation across all expansion states from 1X to 1.8X diameter for the expandable prototype design.

In vivo proof-of-concept of valve expansion: growing lamb model

Seven Polypay and Hampshire breed juvenile sheep (male and non-pregnant female) were included in this study (mean weight = 22.5 ± 0.9 kg, mean age = 9 ± 3 weeks). Experiments were conducted in compliance with the National Institutes of Health (NIH) Guide for the Care and Use of Laboratory Animals. All studies were conducted at the University of Minnesota, Experimental Surgical Services animal facility. The experimental protocol was approved by the University of Minnesota's Institutional Animal Care and Use Committee (1810A36420).

Valve implantation

The expandable biomimetic valve prototype (fig. S13) was implanted in all seven lambs, with a sleeve/sewing cuff constructed with Gore-Tex vascular graft (W.L Gore and Associates, Inc.) to facilitate surgical implantation. Each valve had an internal diameter of 12.5 mm at

implantation. The mean native pulmonary valve annulus diameter was 17 ± 1.4mm among the seven study animals.

All animals were acclimated in the holding facilities for a minimum of three days prior to study initiation. Solid food was withheld for 12 to 24 hours prior to surgery. Water was available at all times for fasting animals. Anesthesia was induced with propofol (2-6 mg/kg, intravenous), ketamine (10 mg/kg, intramuscular), and atropine (0.04 mg/kg, intramuscular). Animals were intubated post induction, and mechanical ventilation was initiated at 9-15 breaths per minute. Isoflurane (1-3%) was administered to maintain anesthesia. EKG monitoring leads were positioned on the animal's limbs. End tidal CO_2, oxygen saturation (SpO_2), and temperature were monitored throughout the procedure. The chest was scrubbed with iodine surgical scrub, patted dry with sterile toweling, and sprayed with iodine/alcohol solution. Once the animal reached a deep plane of anesthesia, 0.4 to 0.8 mg/kg of intravenous succinylcholine chloride was administered. A left thoracotomy via the 4^{th} intercostal space was performed to access the heart and pulmonary valve. Next, the external pulmonary valve annulus diameter and main pulmonary artery length were measured. Baseline hemodynamic data were obtained via direct measurement of the right ventricular and pulmonary artery pressures and placement of a perivascular flow probe (Transonics, TS420) around the distal main pulmonary artery. Baseline 2D epicardial echocardiography was performed to measure the native pulmonary valve annulus diameter and assess overall heart function. After administration of heparin (250 IU/kg), arterial and venous cannulation was performed via the descending thoracic aorta and right atrial appendage, respectively. Cardiopulmonary bypass was initiated, and the animal was gradually cooled to 28°C. Under beating heart conditions, the main pulmonary artery was opened to expose the pulmonary valve. The native pulmonary valve leaflets were excised and interrupted 4-0 Prolene sutures (Ethicon) were placed circumferentially into the native pulmonary valve annulus. The sutures were passed through the sewing skirt of the valve and the device was slid down the sutures using conventional surgical technique to implant the valve prototype in the native pulmonary valve position.

After valve implantation, the pulmonary artery was closed, and hemostasis was obtained. Animals were weaned off cardiopulmonary bypass and arterial and venous cannulas were removed. Once the animal was stabilized off cardiopulmonary bypass, protamine was administered at an approximate ratio of 1:1 (mL of protamine: mL of 1000 IU/ml heparin) for heparin reversal. 2-D epicardial echocardiography, including color and continuous wave Doppler echocardiography was performed to establish baseline post-operative valve function.

The pericardium was then approximated with one polyester suture. Prior to closing the thoracotomy, a local nerve block was introduced via intramuscular injection of lidocaine (1-2 mg/kg) and bupivacaine (1-2 mg/kg) at the incision site. The lungs were inflated, and the chest cavity was irrigated with warm saline antibiotic solution (1 gram of ampicillin in 1 liter of sterile saline). A chest tube was placed for drainage and the chest incision was closed. Isoflurane was discontinued following closure of the thoracotomy. Animals were recovered in the OR, with all monitoring lines and chest tubes being removed prior to awakening from anesthesia. The endotracheal tube was removed once the animal had awakened. Once deemed stable, the animal was moved to the post-operative care area for further recovery. Post-operatively, animals received subcutaneous Heparin (1000 IU) once the evening of surgery and then twice daily for 5 days.

Serial transcatheter balloon dilation of valve implant

To accommodate somatic growth, the animals underwent transcatheter valve dilation procedures at predetermined time points during the survival period. At 2, 6- and 8- weeks post-implant, each animal underwent angiographic studies with transcatheter balloon dilation of the valve device. The extent of valve expansion was the same at each time point across all study animals; the valve was expanded to 16 mm ID at balloon dilation procedure 1 (2 weeks post implant), 18 mm ID at balloon dilation procedure 2 (6 weeks post implant), and 20 mm ID at balloon dilation procedure 3 (8 weeks post implant).

The animals were fasted for 12 to 24 hours (drinking water available at all times during fasting) in preparation for the valve dilation procedure. Anesthetic induction was achieved with propofol (2-6 mg/kg, intravenous), ketamine (10 mg/kg, intramuscular) and atropine (0.04 mg/kg, intramuscular). Animals were intubated post induction, and mechanical ventilation was initiated at 9-15 breaths per minute. Isoflurane (1-3%) was administered as needed to maintain deep anesthesia. EKG monitoring leads were positioned on the animal's limbs. End tidal CO_2, oxygen saturation (SpO_2) and temperature were monitored throughout the procedure. Animals received one dose of intravenous ceftiofur (3 mg/kg) at the start of the procedure.

A small incision was made in the lateral neck to expose the right jugular vein and allow placement of a 14 Fr introducer sheath. Intravenous heparin (250 mg/kg) was administered and a Swan-Ganz catheter was inserted to measure transvalvular pressure gradient and cardiac output prior to valve dilation. To assess valve function, a pigtail catheter was inserted, and right ventricular and main pulmonary artery angiography was performed via injection of contrast and visualization under fluoroscopy. A guide wire was then introduced and an appropriately sized percutaneous balloon catheter (Atlas PTA Balloon Dilation Catheter, Bard Peripheral Vascular Inc.) was advanced into position across the valve device. Under direct fluoroscopic visualization, the balloon was inflated to a nominal pressure of 6 atmospheres to expand the valve. Two dilations were generally performed, with the balloon first positioned distally and then proximally along the length of the device to ensure symmetric valve expansion. Valve performance and heart function were assessed post-dilation via right ventricular and main pulmonary artery angiogram and repeat measurement of transvalvular pressure gradient and cardiac output. Once data collection was completed, the introducer sheath was removed from the jugular vein and the incision was closed. Protamine (intravenous, 1mL: 1mL heparin) was administered at the end of the procedure. After each valve dilation, animals received short-term anticoagulation with one dose of subcutaneous Heparin (1000 IU) administered the evening of the procedure and twice daily administration for two days thereafter.

Echocardiography

Interval transthoracic echocardiography was performed to assess valve hemodynamic performance and overall heart function in the week prior to and following each scheduled balloon dilation procedure. During this procedure the animals received intramuscular injection of acepromazine (0.05 mg/kg) and butorphanol (0.2-0.4 mg/kg) for sedation. Animals were manually restrained and held in left lateral recumbency to allow for suitable imaging. 2D echocardiography, including color and continuous wave Doppler imaging was used to assess valve function, including transvalvular flow velocity and transvalvular peak gradient (mmHg).

Term procedure

At the scheduled term date, animals were placed under anesthesia using the aforementioned regimen. Intracardiac hemodynamic measurements and angiographic imaging were obtained, as previously described. A right thoracotomy (4^{th} intercostal space) incision was then performed to expose the heart. 2D epicardial echocardiography (including color and continuous wave Doppler echocardiography) was performed to assess function of the valve device and overall heart function. After data collection, the animals were euthanized by intravenous injection of phenytoin/pentobarbital solution (Beuthanasia→-D, 87 mg/kg). Necropsy was performed for all study animals, with examination of the heart and valve implant. Gross pathological findings were also examined in the kidneys, lungs, brain, liver, spleen and gastrointestinal tract.

Histological analysis

Explanted valves and the attached pulmonary artery tissue were sent as block specimens (valve and adjacent pulmonary artery wall) for plastic processing and embedding. The device and surrounding tissue were dehydrated in a graded series of ethanol, then infiltrated and embedded in Spurr plastic resin. After polymerization, the device block was sectioned.

The specimen block was first sectioned longitudinally, as shown in Fig. 6B. This section was cut in the center of the valve, perpendicular to the free edge of the two leaflets. The longitudinal section was stained with Hematoxylin and Eosin and Miller's elastic stain.

Next, the valve was transversely sectioned, as shown in Fig. 6B. Sections were cut in the proximal, middle and distal segments of the valve. The proximal and mid sections incorporated the leaflet-frame attachment point at the valve base. The distal section incorporated the attachment point of the leaflets to the distal frame. The transverse sections were stained with Hematoxylin and eosin.

Supplementary Figures

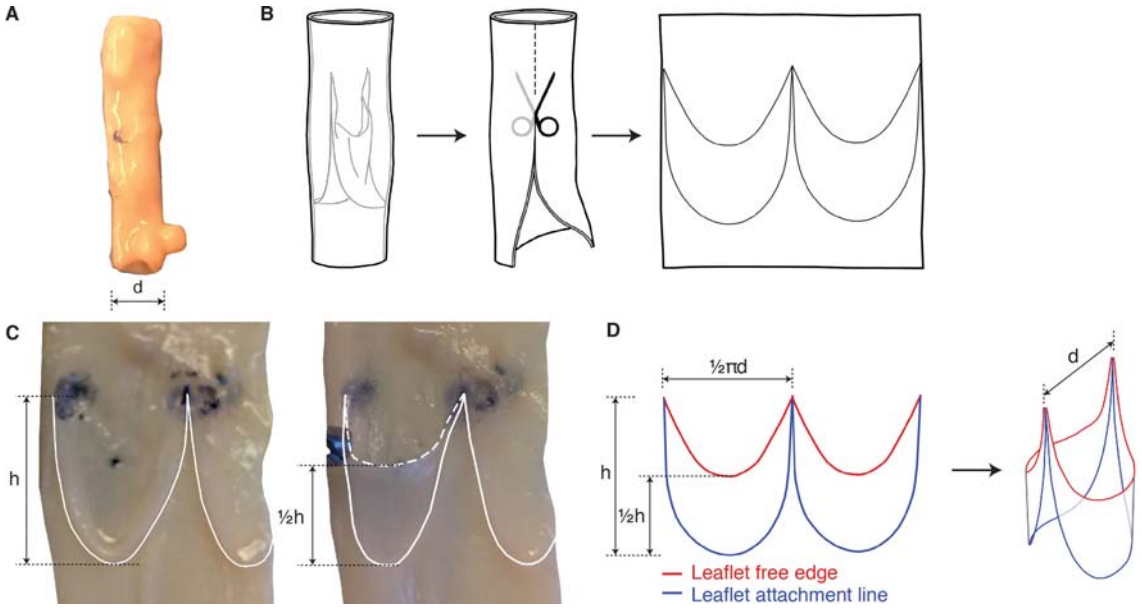

Fig. S1. Determination of human venous valve geometry and dimensions. (A) Photograph of human saphenous vein specimen, **(B)** method of vein dissection to expose venous valve, **(C)** photograph of unrolled human venous valve specimen with outline of leaflet-vessel wall attachment and leaflet free edge (dotted line), and **(D)** key dimensions and geometric features of human venous valve used to inform biomimetic valve design.

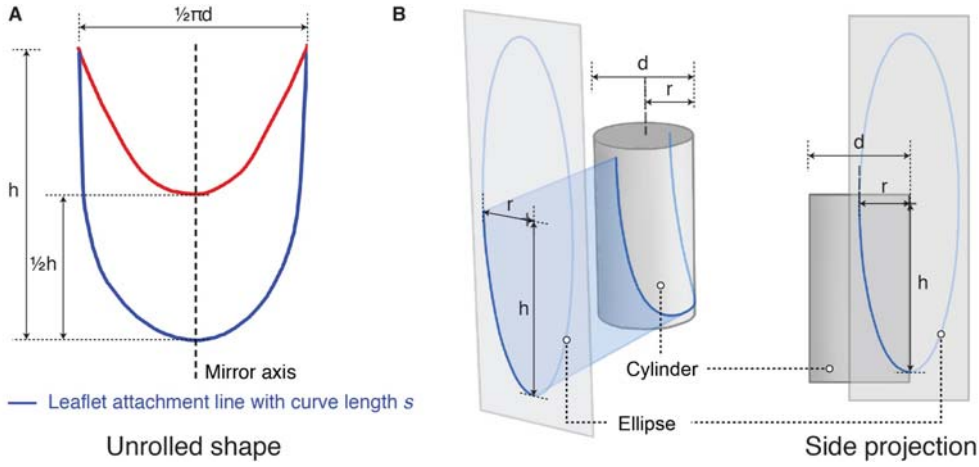

Fig. S2. Methodology for creating biomimetic primary valve geometry. (A) Leaflet profile geometry. **(B)** Geometrical projection of elliptical quadrant on to cylinder to create 3-dimensional leaflet attachment geometry

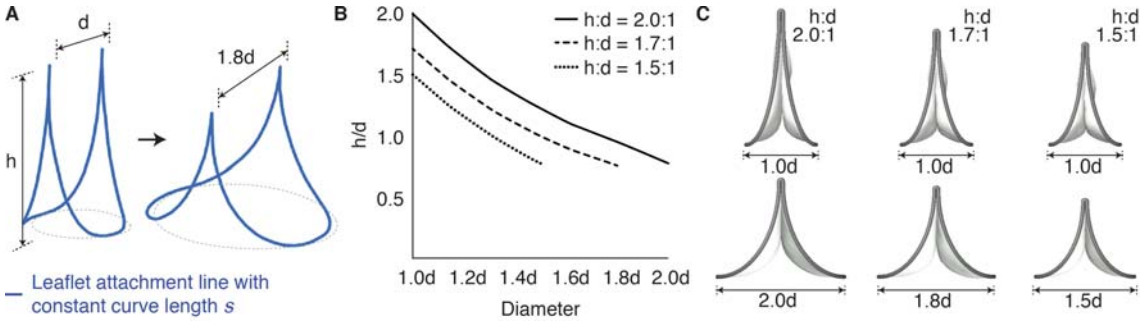

Fig. S3. Expanding valve geometry. (A) Methodology for expanding leaflet attachment geometry of initial height-to-diameter ratio by constraining perimeter length. **(B)** Height-to-diameter ratio change as a function of fixed length leaflet attachment geometry diameter. (**C**) Baseline aspect ratio determines extent of functional valve expansion.

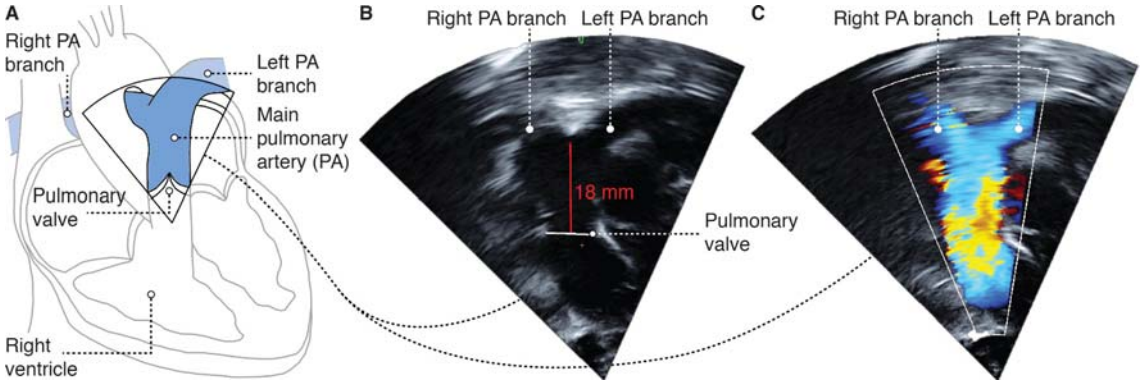

Fig. S4. Determination of optimal valve dimensions for pediatric patients: Echocardiographic imaging of infants with tetralogy of Fallot. (A) Illustration showing echocardiographic view of an infant heart, **(B)** representative 2D echocardiographic image illustrating the pulmonary artery dimensions, and **(C)** corresponding 2D echocardiographic image with color flow doppler.

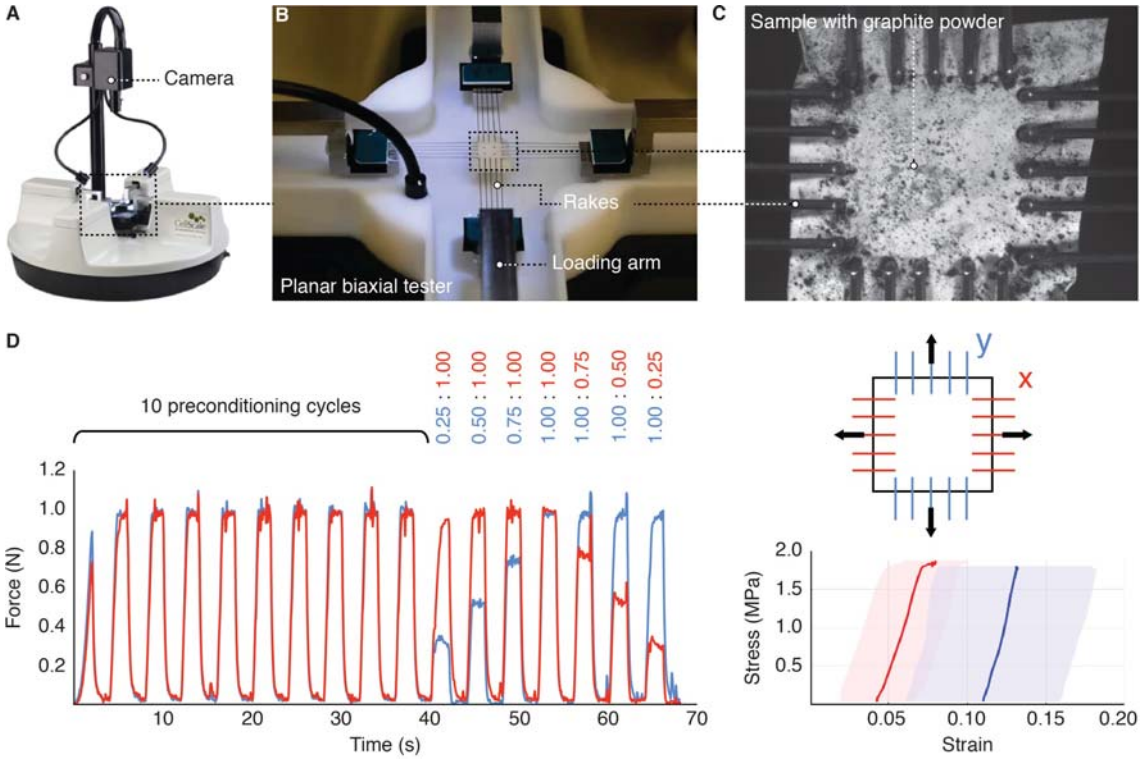

Fig. S5. Experimental setup for biaxial testing of 0.1-mm ePTFE leaflet material. (**A** and **B**) Photographs of biaxial testing machine and details of loading assembly and tungsten rakes. (**C**) View of a 0.1 mm thickness ePTFE (Gore Preclude pericardial membrane, W.L Gore and Associates, Inc.) sample being tested. Cartesian coordinate system indicates positioning of sample based on principal material direction. (**D**) Force-controlled test protocol for assessment of biaxial strain. Corresponding stress-strain plot for 0.1 mm thickness ePTFE at 1 N equibiaxial loading. Stress is represented using second Piola-Kirchhoff membrane tension (N/m), strain is based on Green strain, and the shaded bands indicate (± 2 STD).

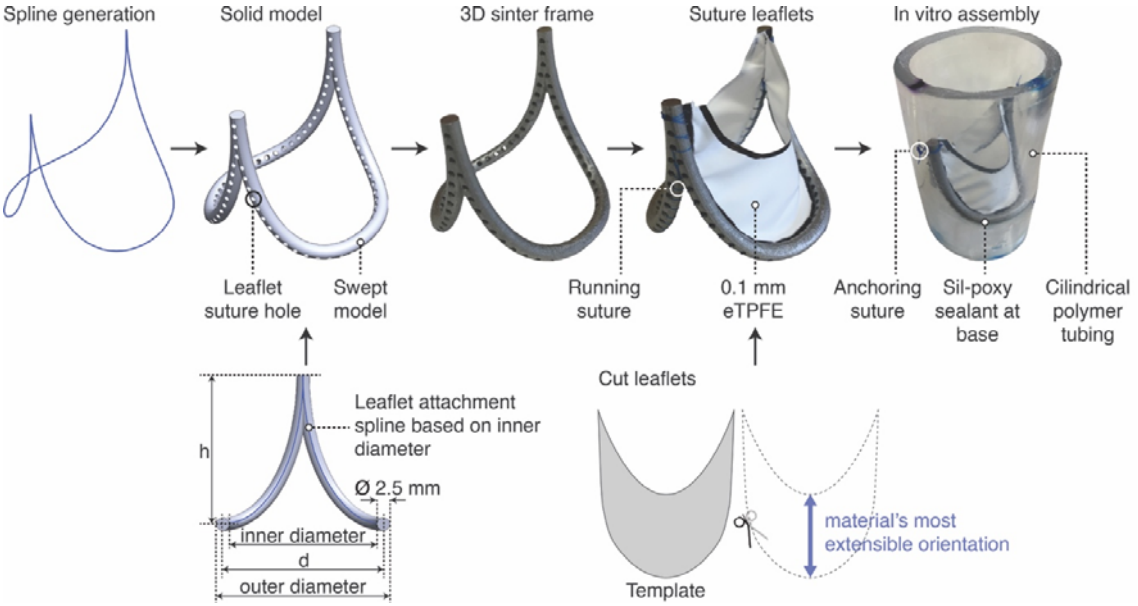

Fig. S6. Fabrication of primary biomimetic valve prototype for in vitro testing. Methodology for creating a sample of the primary biomimetic valve geometry, from initial geometric definition through to a physical embodiment for in vitro testing.

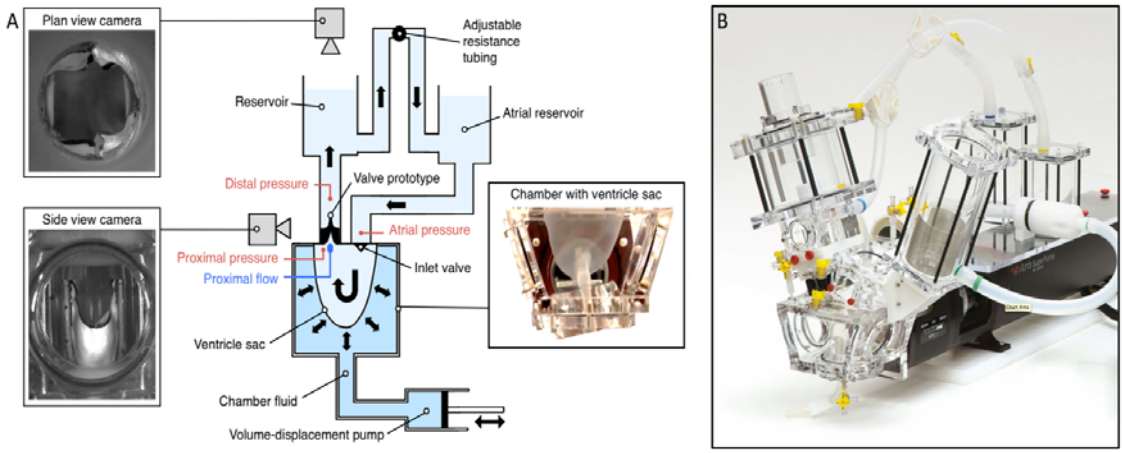

Fig. S7. In vitro circulatory flow loop system. (A) Photographs and schematic representation of the in vitro flow loop apparatus and **(B)** photograph of the in vitro flow loop apparatus (ViVitro Labs Inc).

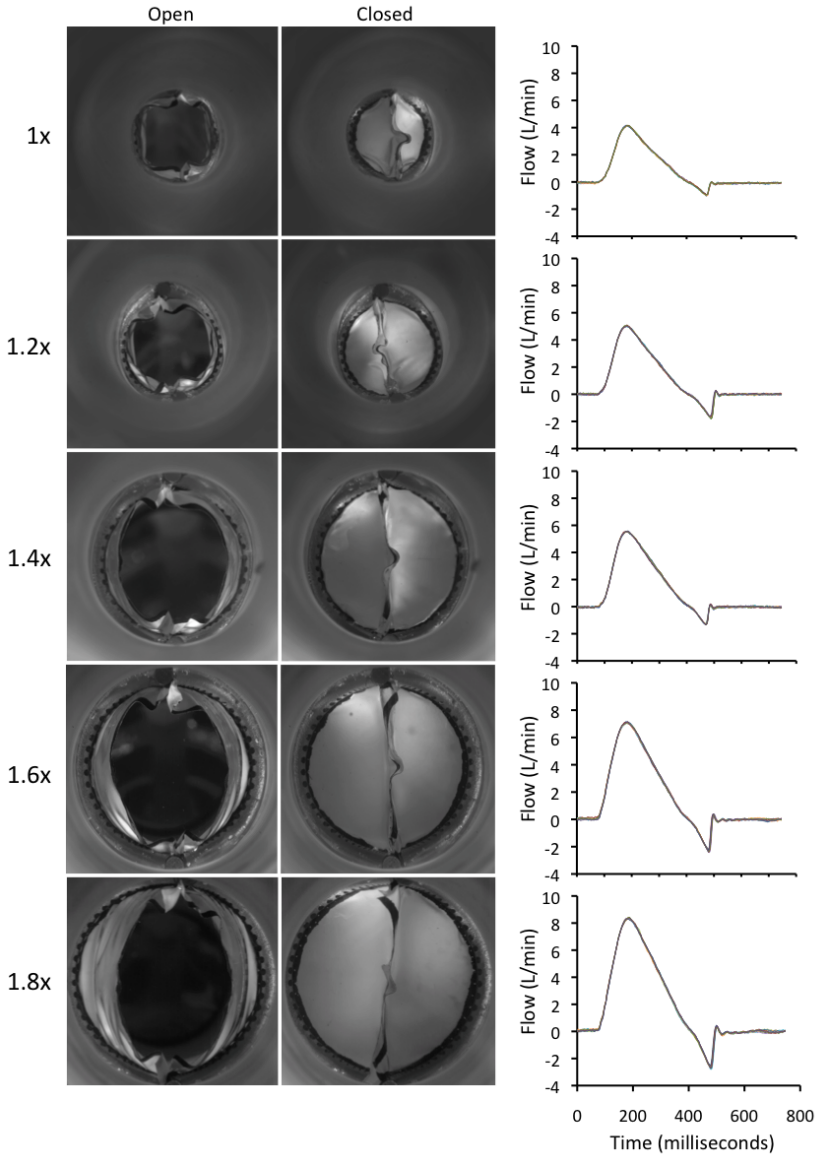

Fig. S8. In vitro flow loop testing data: Primary valve geometry. (**Left)** Photographs of valve prototype at increasing states of expansion (1X up to 1.8X), shown in systole (open valve) and diastole (closed valve). **(Right)** Flow profiles for each valve diameter tested at a cardiac index of 3.0, beat rates/min: 80, systolic duration: 45%. Each plot shows the flow waveform recorded over 10 consecutive cycles, which are overlaid to demonstrate repeatability.

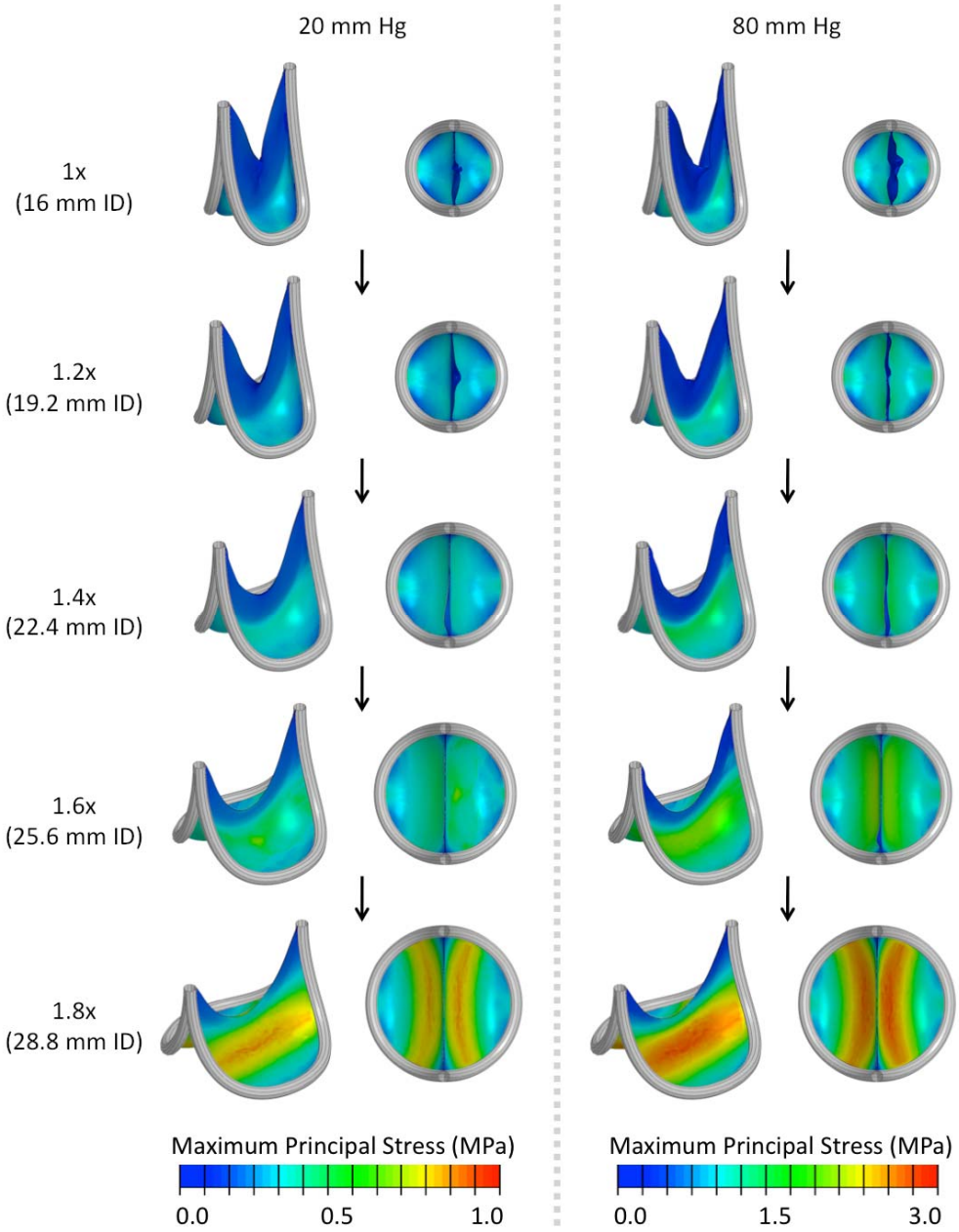

Fig. S9. FE model of leaflet stresses in quasi-static loaded state under right and left heart loading conditions. Leaflet material is 0.1 mm thickness ePTFE (Gore Preclude pericardial membrane, W.L Gore and Associates, Inc.). Results shown are simulated under right heart (20 mmHg, left panel), and left heart (80 mmHg, right panel) loads. All plots are based on the same scale of maximum principal stress, ranging between 0 to 1 MPa and 0 to 3 MPa for right and left heart loads, respectively.

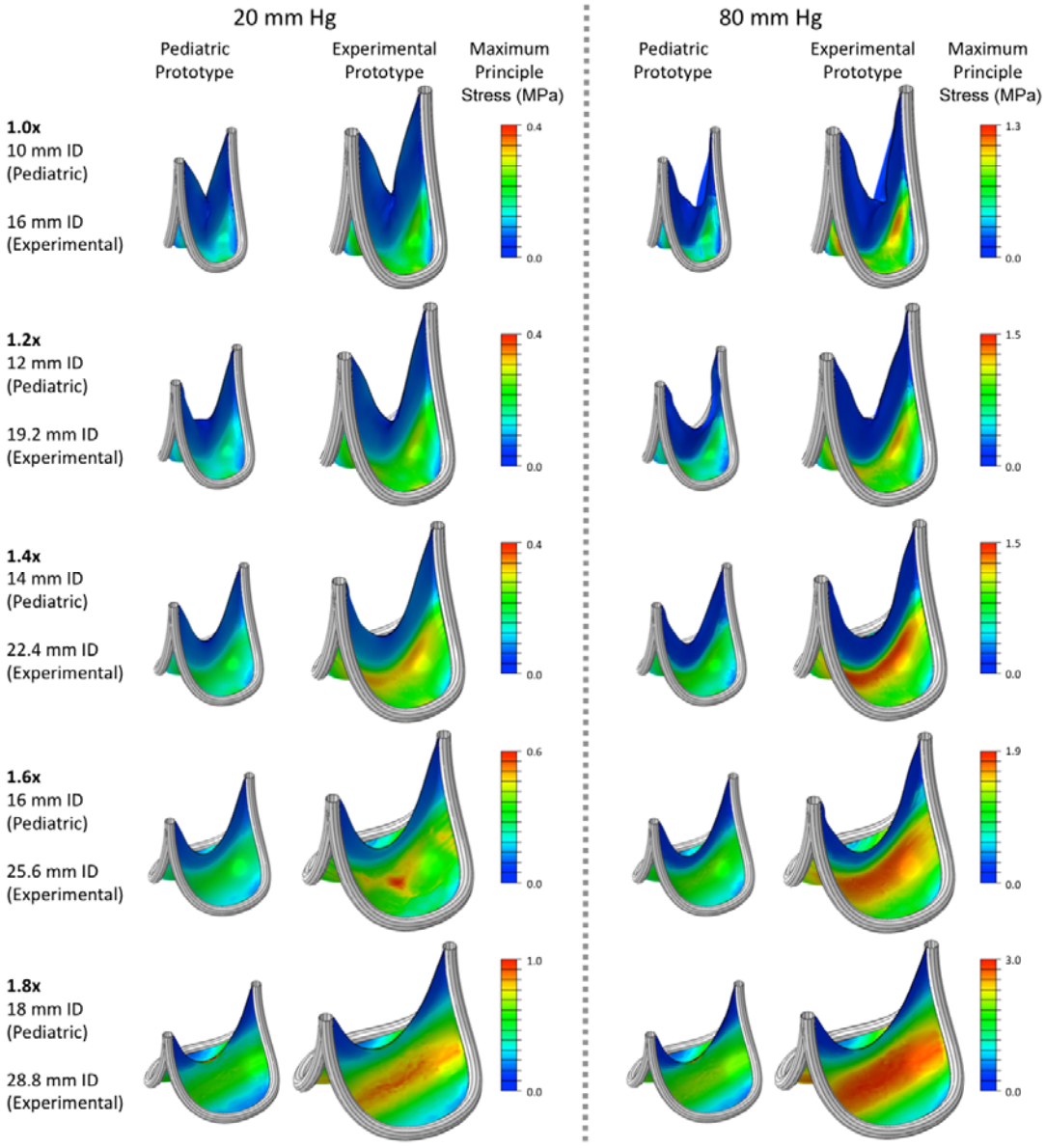

Fig. S10. FE model of leaflet stresses in quasi-static loaded state under right and left heart conditions—Pediatric dimensions. Leaflet material is 0.1 mm thickness ePTFE (Gore Preclude pericardial membrane, W.L Gore and Associates, Inc.). Results shown are simulated under right heart (20 mmHg, left panel), and left heart (80 mmHg, right panel) loads. All plots are based on the same scale of maximum principal stress, ranging between 0 to 1 MPa and 0 to 3 MPa for right and left heart loads, respectively.

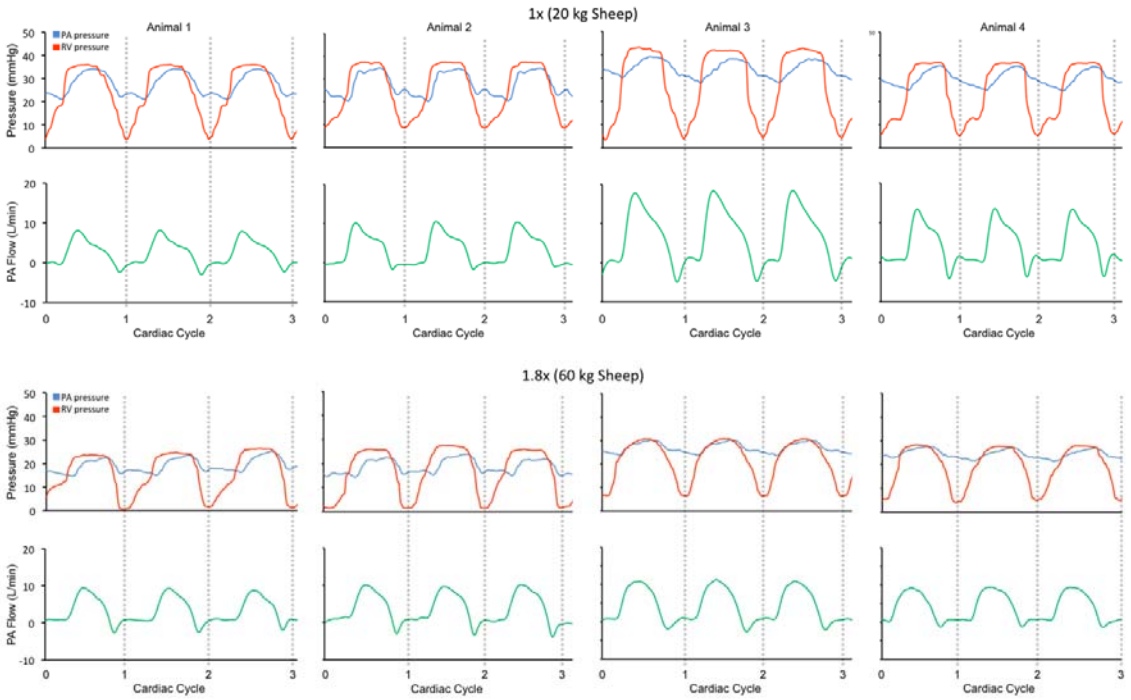

Fig. S11. Acute in vivo studies in juvenile and adult sheep: Representative hemodynamic data. Representative in vivo data obtained from all 8 study animals showing **right ventricular and pulmonary artery pressures** and pulmonary artery flow for the 1X and 1.8X expanded valve geometries, respectively. RV = right ventricular, PA = pulmonary artery.

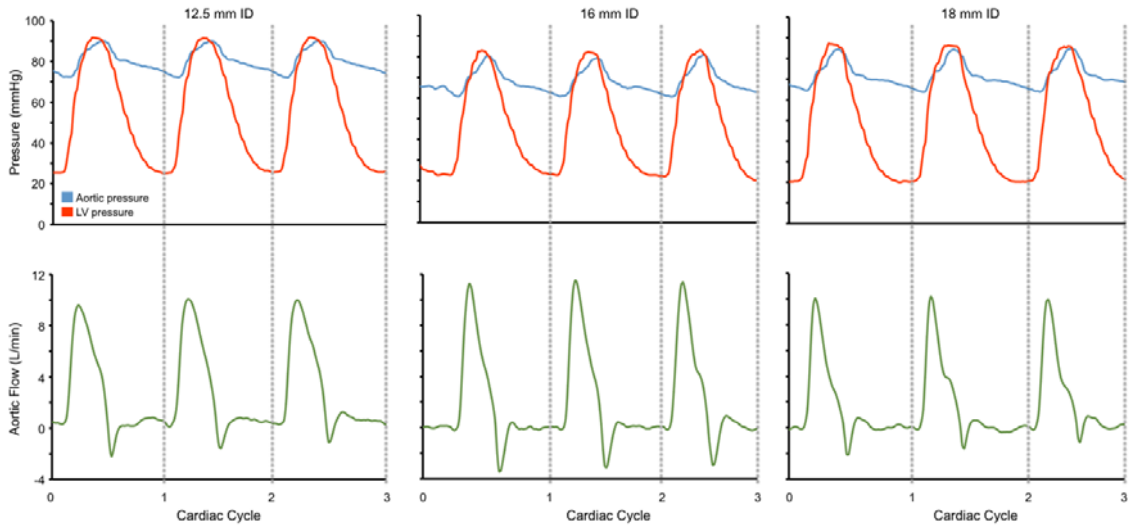

Fig. S12. In vivo validation of biomimetic valve performance in the native aortic valve position: Acute studies in juvenile sheep. Representative in vivo data obtained from one study animal demonstrating left ventricular and aortic pressures and ascending aortic flow for the 12.5 mm ID, 16 mm ID and 18 mm ID expansion states, respectively. LV = left ventricle.

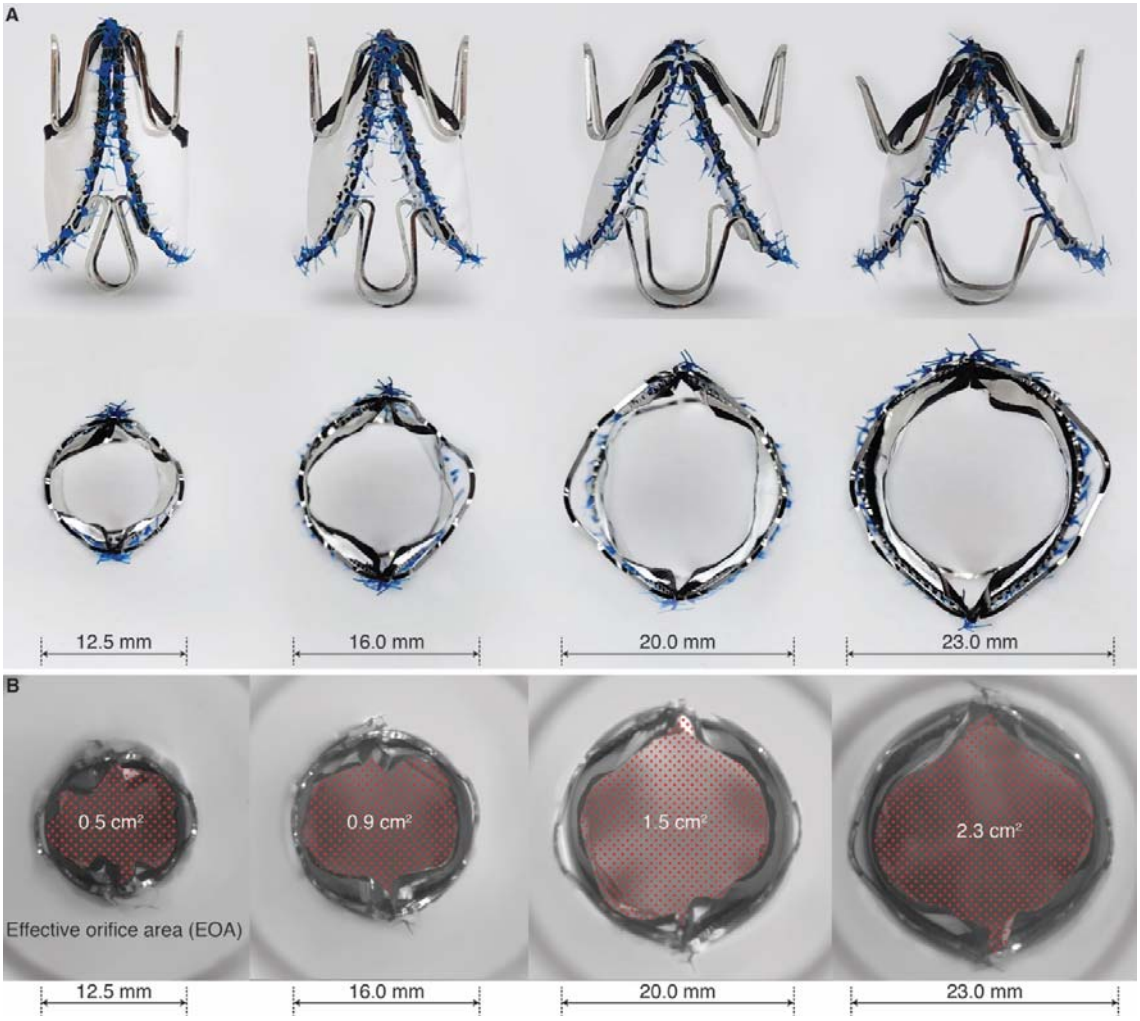

Fig. S13. Expandable biomimetic valve prototype: Frame expansion profile and leaflet opening function. (A) Side view photographs of fabricated expandable biomimetic valve prototype, with 0.1 mm thick ePTFE leaflets sewn to the stainless-steel stent. Photographs show serial expansion of valve from 12.5 mm ID (1X) to 23 mm ID (1.8X). (**B**) Corresponding top view images of valve outflow surface from 1X to 1.8X diameter. (**C**) Photographs of valves being testing in in vitro flow loop system. Leaflets are in the open position, and the red dots indicate effective orifice area of valve at each stage of expansion. Effective orifice area (EOA, cm^2) = Qrms / (51.6 $\sqrt{(\Delta P/\rho)}$).

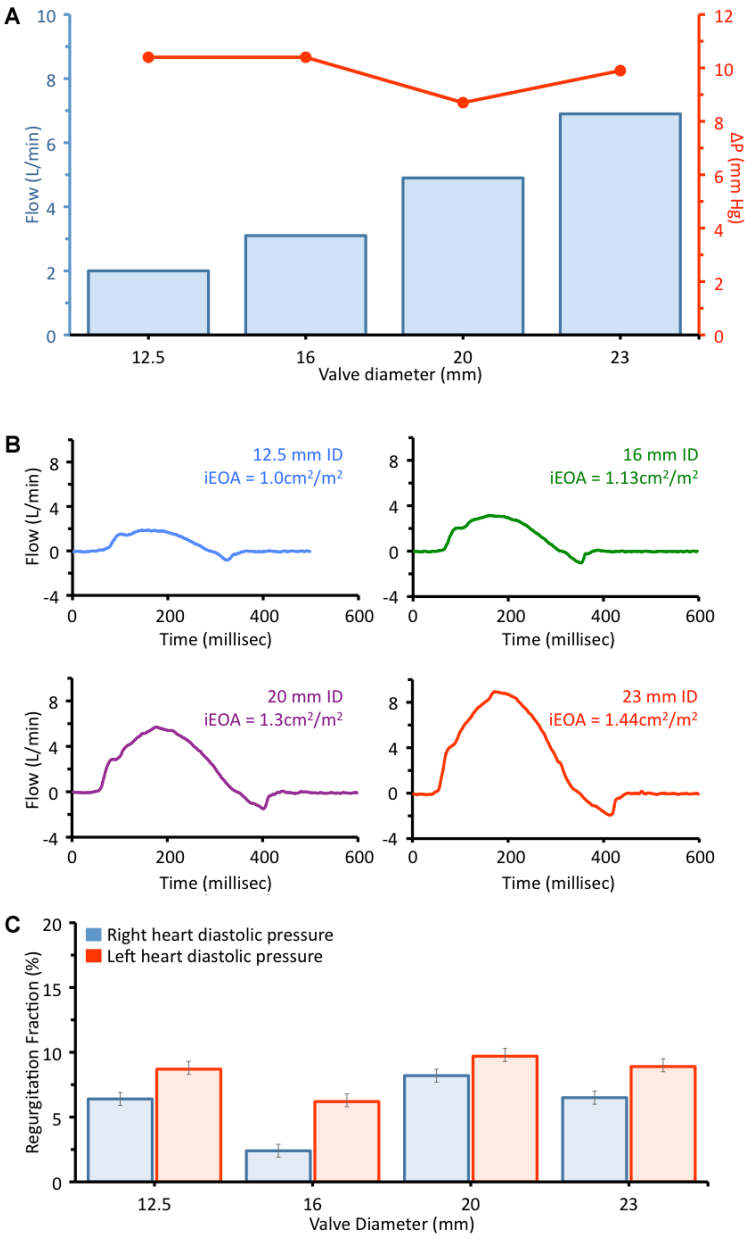

Fig. S14. In vitro characterization of the biomimetic expandable valve: Flow loop testing. (A, B, C) Expandable valve prototype was tested at different states of diametric expansion (1X to 1.8X) in an in vitro circulatory flow loop, under physiologic left and right heart conditions. **(A)** Mean transvalvular (ΔP) pressure gradient (red line) at each stage of valve expansion (1X to 1.8X). Flow is adjusted to match valve size and replicate the physiology of a growing child. **(B)** Four plots demonstrate flow profiles of the expanding valve geometry from 1X (12.5 mm ID) to 1.8X (23 mm ID). **(C)** Valve competence (closing function) under right (20 mmHg, blue bars) and left (80 mmHg, red bars) heart loads. Error bars represent ±1 standard deviation.

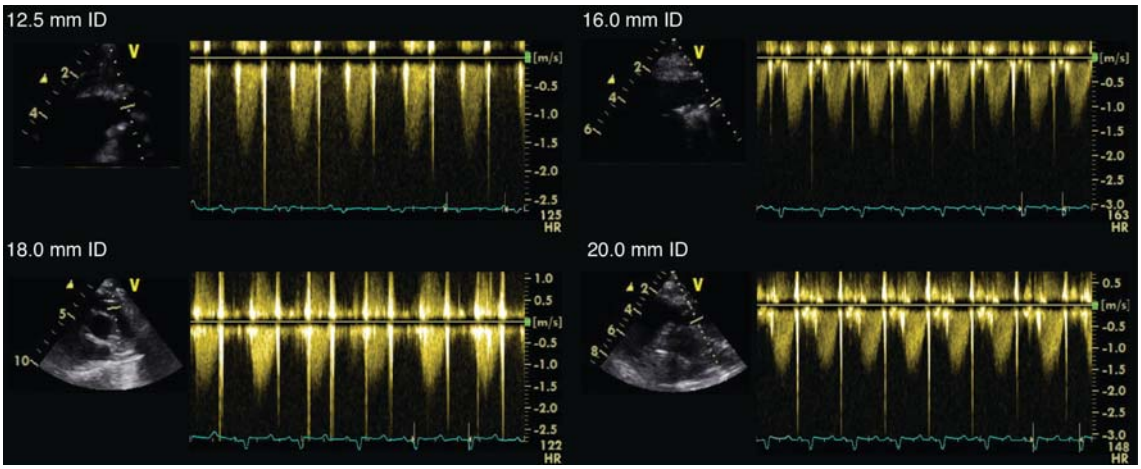

Fig. S15. Serial echocardiograms measuring transvalvular gradient in growing lambs. Representative 2D transthoracic echocardiographic images demonstrating continuous wave Doppler measurement of peak transvalvular flow velocity at each state of device expansion during the 10-week survival period.

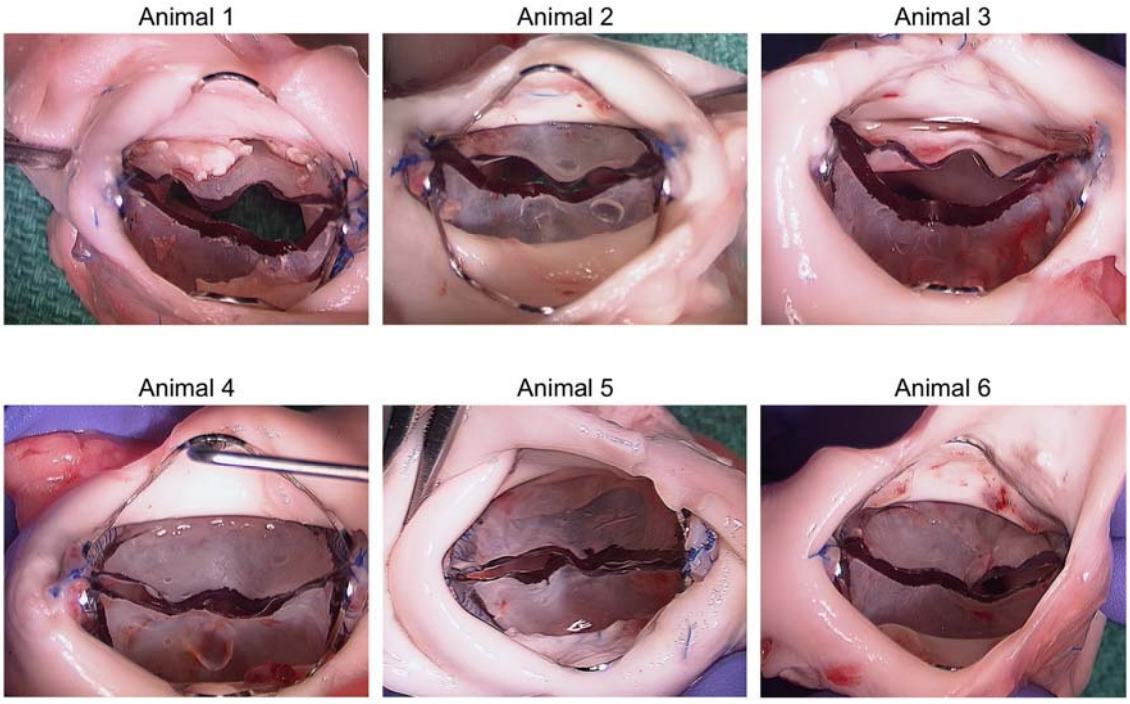

Fig. S16. Macroscopic appearance of biomimetic expandable valve at time of explant in six study animals. Images of valve outflow surface in six survival study animals at term procedure (9 - 10 weeks post implant). NB: Outflow view of study animal No. 7 is shown in the manuscript, Fig. 6A)

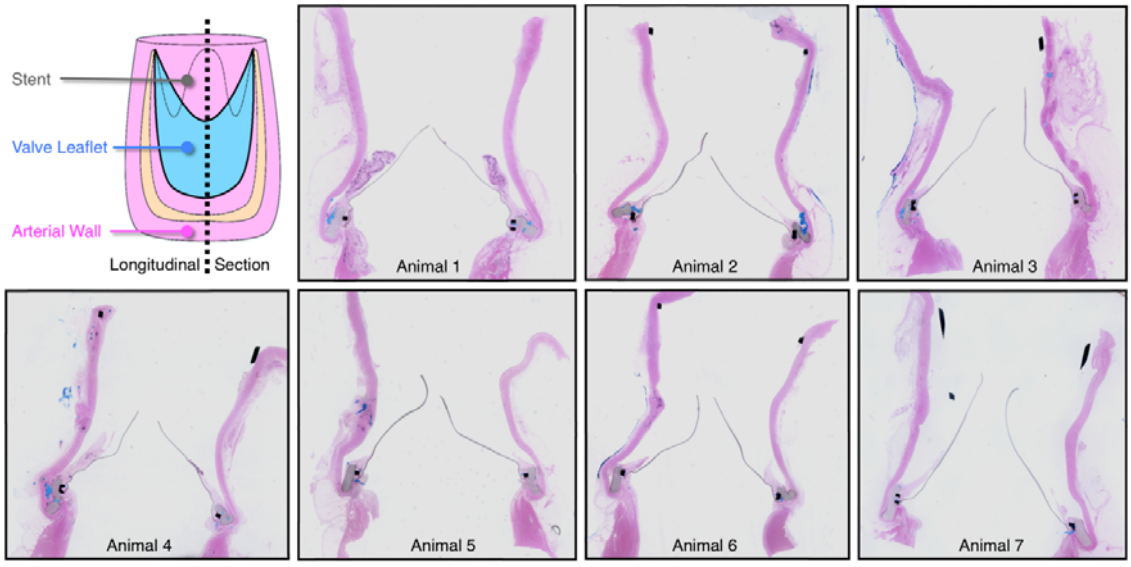

Fig. S17. Histological profile of biomimetic expandable valve prototype at time of explant (63-68 days post implantation). Hematoxylin and Eosin (H&E) stained longitudinal sections from all 7 study animals. All images measure approximately 30 mm in width.

Supplementary Tables

Table S1. Native human venous valve measurements.

Human venous valve specimen	Valve height (mm)	Valve diameter (mm)	Valve height: diameter ratio	Leaflet mid-height (mm)	Leaflet mid-height: overall height ratio
1	16	8	2:1	8	0.5:1
2	17	8	2.125:1	8	0.47:1
3	6	3	2:1	3	0.5:1
4	6	3	2:1	3	0.5:1

Table S2. Peak-to-peak transvalvular pressure gradient for 1× valve geometry in four animals. Data based on n = 10 consecutive cardiac cycles at ~2 hours post device implant.

	Mean (mmHg)	Standard deviation (mmHg)
Study 1	1.5	0.4
Study 2	2.9	0.3
Study 3	3.1	0.7
Study 4	0.9	0.5

Table S3. Peak-to-peak transvalvular pressure gradient for 1.8× expanded valve geometry in four animals. Data based on n = 10 consecutive cardiac cycles at ~2 hours post device implant.

	Mean (mmHg)	Standard deviation (mmHg)
Study 1	1.5	0.2
Study 2	3.8	0.2
Study 3	0.6	0.3
Study 4	1.3	0.2

Table S4. Regurgitant fraction for 1× valve geometry in four animals. Data based on n = 10 consecutive cardiac cycles at ~2 hours post device implant

	Mean	Standard deviation
Study 1	5.3%	0.8%
Study 2	7.9%	2.0%
Study 3	4.7%	1.3%
Study 4	4.4%	1.3%

Table S5. Regurgitant fraction for 1.8× expanded valve geometry in four animals. Data based on n = 10 consecutive cardiac cycles at ~2 hours post device implant.

	Mean	Standard deviation
Study 1	10.3%	2.2%
Study 2	11.3%	1.6%
Study 3	7.0%	0.8%
Study 4	5.8%	0.7%

Table S6. In vivo hemodynamic data for seven survival study animals at four separate time points. BD = valve balloon dilation. BD 1 = 12.5 mm to 16 mm ID (2 weeks post implant), BD 2 = 16 mm to 18 mm ID (6 weeks post implant), BD 3 = 18 mm to 20 mm ID (8-9 weeks post implant), Term = one-week post BD 3.

		Pre-dilation hemodynamic data				**Post-dilation hemodynamic data**			
Animal #	**Dilation #**	**RVp** (mmHg)	**PAp** (mmHg)	**ΔP** (mmHg)	**CO** (L/min)	**RVp** (mmHg)	**PAp** (mmHg)	**ΔP** (mmHg)	**CO** (L/min)
1	BD 1	47/6	18/9	29	2.3	48/5	22/9	26	2.8
	BD 2	28/5	18/8	10	2.6	23/5	18/8	5	2.6
	BD 3	18/0	15/4	3	2.5	16/2	12/4	4	2.5
	Term	18/9	16/10	2	3.5				
2	BD 1	38/3	15/5	23	3.2	31/0	19/6	12	3.6
	BD 2	32/5	19/9	13	4.1	32/6	19/7	13	5.2
	BD 3	22/5	12/6	10	3.2	17/3	12/7	5	4.2
	Term	20/2	14/5	6	2.6				
3	BD 1	33/2	14/6	19	2.9	32/5	26/8	6	3.5
	BD 2	24/2	16/8	8	5.1	27/4	16/11	11	6.4
	BD 3	24/10	17/11	7	2.8	22/7	14/10	8	3.8
	Term	21/9	20/13	1	3.4				
4	BD 1	41/9	20/18	21	3.1	34/12	19/15	15	3.9
	BD 2	43/2	21/13	22	5.4	40/9	23/19	17	7.5
	BD 3	25/5	16/9	9	4.3	28/5	17/8	11	5.5
	Term	33/3	15/12	18	6.2				
5	BD 1	28/1	8/5	20	4.2	24/2	15/4	9	4.6
	BD 2	42/9	16/11	26	5.1	36/6	19/10	17	7.6
	BD 3	25/3	14/6	11	5.2	28/2	14/6	14	6.5
	Term	29/0	19/10	10	5.7				
6	BD 1	22/4	12 / 5	10	3.2	23/2	13/3	10	3.4
	BD 2	30/0	15/9	15	3.2	33/0	23/14	10	3.3
	BD 3	25/0	16/10	9	4.6	22/0	13/10	9	5.2
	Term	27/0	13/7	8	5.9				
7	BD 1	33/0	10/5	23	3.3	31/1	13/6	18	3.6
	BD 2	32/5	17/9	15	3.9	37/4	20/13	17	4.5
	BD 3	29/0	13/9	16	4.7	24/0	13/5	11	5.1
	Term	30/3	17/7	13	5.9				

Table S7. 2D echocardiogram-derived transvalvular peak gradient at all valve expansion states. The peak transvalvular gradient (mmHg) as measured by continuous wave doppler (CWD) is reported at each stage of valve expansion from 12.5 mm to 20 mm internal diameter (ID) in all 7 survival study animals throughout the 9-10 week survival period.

	Valve internal diameter (ID)			
Animal #	**12.5 mm** Peak gradient (mmHg)	**16mm ID** Peak gradient (mmHg)	**18 mm ID** Peak gradient (mmHg	**20 mm ID** Peak gradient (mmHg)
1	17.8	5.5	7.8	11.2
2	36.3	14.4	20.5	14.1
3	22.4	17.7	14.4	13.5
4	25.6	24.4	17.9	15.7
5	22.3	16.5	19.9	12.9
6	12.9	13.3	10.8	12.4
7	18.1	20.6	13.1	13.2
Mean	22.2	16.1	14.9	13.3
Stdev	± 7.5	± 6.0	± 4.8	± 1.4

Movie S1. A Geometrically adaptable heart valve replacement. In this video, we demonstrate the venous valve inspired biomimetic valve design using 3-dimensional models of the native human venous valve expanding under physiologic volume loads and its geometrically adaptable bileaflet valve analogue. We demonstrate functionality of the primary biomimetic valve design with footage of the expanding valve geometry in an in vitro flow loop system, and we show the results of finite element simulations evaluating the magnitude and distribution of stresses across the closed and loaded valve leaflet at various states of valve expansion. We present echocardiographic color Doppler images demonstrating laminar flow along the length of the valve and into the branch pulmonary arteries. Then, we demonstrate in vivo valve expansion in a growing animal, with representative footage of a balloon expansion procedure in a juvenile sheep at two weeks post valve implantation. This is followed by representative right ventricular angiograms performed at two- and seven-weeks post valve implantation, demonstrating successful valve expansion to accommodate growth. Finally, we provide echocardiographic (ultrasound) evidence of the biomimetic bileaflet valve flow dynamics obtained during acute and long-term in vivo studies, with representative epicardial echocardiogram color doppler images showing prominent flow recirculation around the valve periphery during the valve opening phase. This flow pattern we demonstrate on both short and long-axis echocardiographic views.